J Mater Sci (2006) 41:7119–7129
DOI 10.1007/s10853-006-0932-8

Structural characterization of a novel spatially coherent crystalline nanocomposite obtained from a melt of KBr, RbCl, RbBr, KI and RbI salts

A. E. Cordero-Borboa · R. R. Mijangos · P. S. Schabes-Retchkiman

Received: 22 June 2005 / Accepted: 27 December 2005 / Published online: 12 October 2006
© Springer Science+Business Media, LLC 2006

Abstract Large transparent bulks, grown by a pulling technique from a melt prepared by mixing equal molar fractions of KBr, RbCl, RbBr, KI and RbI salts, are characterized by X-ray diffractometry, Laue photography and low-current-field-emission high-resolution electron microscopy. The bulks consist of a multiphase crystalline material made of nanocrystallites (with a size distribution range of 5–60 nm) of three different fcc-phases. One of these phases is identified as single RbBr while the other two are discussed to be binary KI(39%):RbI(61%) and ternary KBr(47%): RbCl(39%):RbBr(14%), respectively, with unit-cell sizes of 6.889 ± 0.007, 7.234 ± 0.025 and 6.631 ± 0.005 Å, respectively. The lattices of the crystallites, no matter the particular phase they belong to, are spatially coherent to each other so that the normal vectors to a lattice (HKL)-plane, in different crystallites, are confined in the space within a narrow circular cone around the lattice [HKL]-direction. For this cone, the semi-apical angle was determined for the cases of HKL equal to 301, 411, 331, 401, 311, 511, 221 and 321. The ternary phase crystallites contribute mainly to the observed departure of the composite crystallographic texture from a condition of full spatial coherence.

A. E. Cordero-Borboa (✉) · P. S. Schabes-Retchkiman
Instituto de Física, Universidad Nacional Autónoma de México, A.P. 20-364, Del. A. Obregón, México DF 01000, México
e-mail: cordero@fisica.unam.mx

R. R. Mijangos
Centro de Investigación en Física, UNISON, A.P. 5-88, Hermosillo 83190, Sonora, México

Introduction

The present report introduces the reader to the obtainment and characterization of spatially-coherent composites made of crystallites of various different mixed alkali-halide phases, and also opens the door to both the study of the physical properties of this type of composites and the use of them as simple structural models in the study of other spatially-coherent multiphase crystalline materials.

Since the early X-ray diffraction studies carried out on rock salt [1] and other alkali halide salts (among them the ones used in the present work as precursor salts [2–8]), alkali-halide crystals have played a central role in the modern study of crystalline materials. In principle, two different isomorphous alkali-halide crystals may be melted together in order to give place by crystallization of the so-obtained melt to a mixed binary alkali-halide material. However, the lattice distortion associated [9, 10] to different ion species replacing to each other during the formation of a binary mixed alkali-halide matrix may be large enough to forbid the formation of a binary continuous random substitutional solid-solution series. A series of this sort is empirically expected [11, 12] to be formed whenever the two salts used to prepare the melt differ in unit-cell size from each other by less than about 10%. Attending to this criterion, only eleven different binary continuous random substitutional solid-solution series may be expected to form, in particular, from the ion species building the alkali halides used as precursor salts in the present work. These series are listed in Table 1 together with their corresponding solid-solution unit-cell-size-range limits. The differences between these limits are also shown in Table 1. All of the series listed

Table 1 Solid-solution unit-cell-size range limits, and their corresponding differences, for the binary alkali-halide systems that satisfy the 10%-unit-cell-size difference criterion and that may in principle be formed by the ion species in the KBr, RbCl, RbBr, KI and RbI salts

Binary system U_x:V_{1-x}	Solid-solution unit-cell-size range limits[a] (Å)		U, V unit-cell-size difference (%)
	$x = 1$	$x = 0$	
KBr:KCl	6.6005	6.291	4.9
KBr:KI	6.6005	7.065	7.0
RbCl:RbBr	6.5810	6.889	4.7
RbI:RbBr	7.342	6.889	6.5
KCl:RbCl	6.291	6.5810	4.6
KBr:RbBr	6.6005	6.889	4.4
KI:RbI	7.065	7.342	4.0
KCl:RbBr	6.2917	6.889	8.7
KI:RbCl	7.065	6.5810	6.9
KI:RbBr	7.065	6.889	2.5
RbCl:KBr	6.5810	6.6005	0.3

[a] Reference [31]

in this table, with the exceptions of KI:RbCl and KI:RbBr, have been currently obtained [12–14] in the laboratory. Results from early X-ray diffraction works carried out [15, 16] on the binary mixed KCl:KBr system showed the fact that a binary mixed alkali-halide crystal obtained from a melt of two isomorphous alkali-halide salts inherits from these salts some lattice geometrical features (e.g. the Bravais lattice type) and behaviours (e.g. the one established by the Vegard's rule). This fact allows the lattice-dimension-depending physical properties of a binary mixed material to be tailored by tuning the relative concentration in this material of the involved alkali-halide components. As a binary mixed alkali-halide material obtained by pulling techniques from a melt of two isomorphous alkali-halide salts is commonly transparent, the influence of the composition of this material on the optical properties of any optically-active singularity existing within its mixed matrix has been of principal concern. In particular, the optical properties of colour centres [17, 18] and divalent cation impurities [19–23] in binary mixed alkali halides have been separately investigated to some extent as a function of the composition of these crystals. Recently, the composition dependence of the optical properties of these two types of singularities, one in the presence of the other, has been investigated [24] in F-coloured Eu^{2+}-doped KCl:KBr crystals. Ternary, quaternary or higher-order mixed alkali halides have been scarcely studied. Mixed ternary KBr:RbCl:KCl and quaternary KBr:RbCl:RbBr:KCl crystalline bulks have been obtained [25, 26] and characterized by X-ray diffractometry [25, 27]. These materials may be described by fcc-lattices whose lattice parameters obey generalized Vegard's rules for ternary and quaternary mixed systems, respectively. The optical properties of colour centres and impurity Eu^{2+}-ions have been also recently studied [27–29] in these materials.

Multiphase crystalline composites consisting of aggregates of crystallites of various different mixed alkali-halide phases have not yet been the subject, as far as the authors are aware, of structural studies, even when these materials are expected to inherit some structural features and behaviours from their separated mixed alkali-halide crystalline phases. Such studies are necessary to be performed as a first step to understand the physical properties of these novel materials, and, also, in order to realize the role that these materials may play, as simple structural models, in the study of other crystalline composites made of various mixed phases.

The present work was undertaken to characterize the crystallographic structure and texture of a multiphase crystalline composite obtained from a melt prepared by mixing pure KBr, RbCl, RbBr, KI and RbI salts. This was done by using X-ray diffractometry (XRD), X-ray Laue-type photography (XRLP) and low-current-field-emission high-resolution electron microscopy (LCFE-HREM). This composite is made of nanocrystallites of three different fcc-phases. From these phases, one is identified as the single RbBr phase, another one is discussed to be a binary mixed alkali-halide phase, and the third one is discussed to be a ternary mixed alkali-halide phase. The compositions of these two mixed phases are proposed. The crystallites forming the composite, no matter the particular phase they belong to, are spatially coherent to each other so that the normals to a lattice (HKL)-plane, in different crystallites, are confined within a narrow circular cone around the lattice [HKL]-direction. The semiapical angle of this cone is determined for different HKL-cases.

Experimental details

Large transparent bulks were obtained (Fig. 1) by the Czochralski technique [30] from a melt at 750 °C prepared by mixing equal molar fractions of pure KBr, RbCl, RbBr, KI and RbI salts. A dry argon atmosphere was maintained inside the growth chamber in order to minimize the contamination by molecules and ions in the air like H_2O, O_2 and OH^-. The bulks were cleaved easily off along their cubic {100}-faces in order to obtain plate-like samples with sizes of about

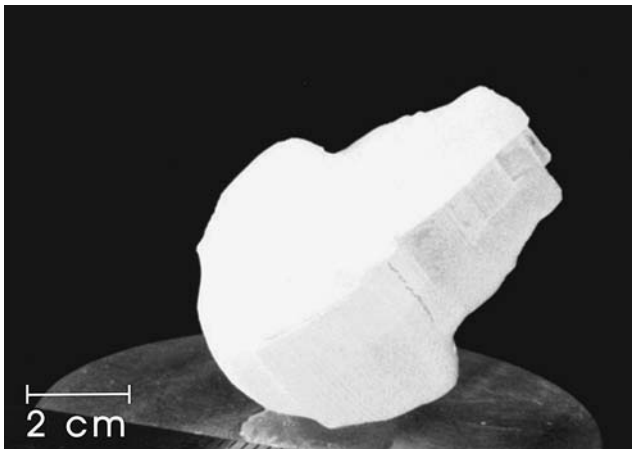

Fig. 1 Photograph of a typical crystal bulk obtained by the Czochralski technique from a melt prepared by mixing equal molar fractions of pure KBr, RbCl, RbBr, KI and RbI salts

$0.1 \times 0.1 \times 0.02$ cm^3 and $1.0 \times 1.0 \times 0.1$ cm^3 for crystallographic texture studies by XRLP and crystal-plate-XRD, respectively. Some fragments were ground to powder in an agate mortar and then mixed with standard silicon (in concentration of about 20% by weight) in order to get suitable specimens for phase identification and unit-cell-size measurements by powder XRD. Diffractograms for texture exploration, phase identification and unit-cell-size measurement purposes were taken using counting times of 1, 4 and 20 s, respectively, per scanning step of 0.02° in twice the Bragg angle (2θ). This was done using a Siemens-D5000 diffractometer equipped with a variable divergence diaphragm, a secondary-arm graphite monochromator and an Cu-anode X-ray tube operated at 30 kV–20 mA. Specimens for crystal-plate XRD were individually analyzed by mounting them onto the diffractometer so that one of their crystal {100}-faces coincided with the sample-cup working plane. Powder XRD-spectra were calibrated in 2θ using a calibration curve that was previously built by plotting the difference between the observed and the expected 2θ-positions for the silicon reflections versus 2θ. The corresponding interplanar distances d were calculated from the calibrated 2θ-values by means of the Bragg's law. Transmission XRLP-patterns were taken along the lattice [001]-direction, using Ni-filtered Cu-radiation and a film-to-specimen distance (D) of 50 mm. To do this, a Charles-Supper-3520 precession camera mounted on a Philips-PW1729 X-ray generator operating at 35 kV–25 mA was used. Thin specimens for examination by LCFE-HREM were obtained by dispersing dry powder of the samples between two glass microscope slides and then picking up some powder grains by touching them with a carbon-coated 3 mm-microscope grid. The specimens were studied in a JEOL-2010 FEG transmission electron microscopy operated at 200 keV and equipped with scanning transmission electron microscopy capabilities, a gattan image filter, image intensifying cameras and annular dark field detectors. As the samples are highly sensitive to electron radiation damage very-low-electron-current high-angle annular dark field images were used to localize the zones to be studied by LCFE-HREM.

Results

Powder XRD

Figure 2 shows a typical powder X-ray diffractogram of a bulk grown from a melt prepared by mixing equal molar fractions of pure KBr, RbCl, RbBr, KI and RbI salts, together with the International Centre for Diffraction Data Powder Diffraction File (ICDD-PDF)

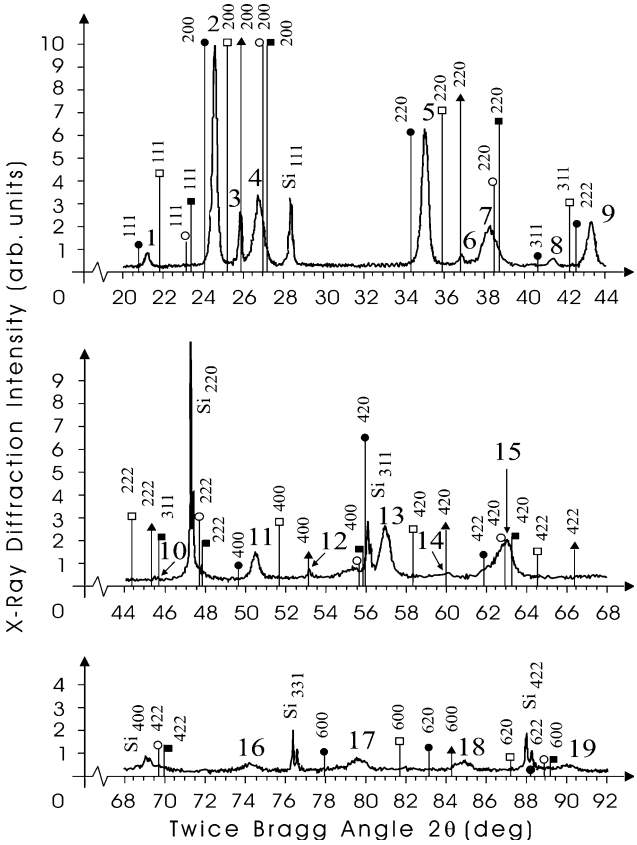

Fig. 2 Powder X-ray diffractogram of the crystal shown in Fig. 1. The diffractogram consists of nineteen well-defined Bragg reflections (1–19) aside from the reflections (Si_{HKL}) corresponding to the internal standard silicon. ICDD-PDF-card lines corresponding to KBr, RbCl, RbBr, KI and RbI (○, ■, ▲, □ and •, respectively) are also shown.

card lines corresponding [31] to these salts. This diffractogram consists of a number of well-defined Bragg reflections (1–19 in the figure) aside from the diffraction peaks corresponding to the internal standard silicon (Si_{HKL} in the figure), showing that the material under characterization is fully crystallized. Some of these reflections (e.g. reflections 3, 6, 10, 12 and 14 in Fig. 2) were found to match in position with the most intense ICDD-PDF-card lines corresponding to the RbBr phase (card lines 200, 220, 222, 400 and 420, respectively, in Fig. 2), and, therefore, this phase (phase S from here on in this paper) was inferred to form part of the sample. For the sake of numerical comparison, the measured interplanar distances and relative intensities for these reflections as well as the corresponding ICDD-PDF-card line values are listed in Table 2. In this table the relative intensities of the experimental reflections do not follow those of the expected pattern based on the standard diffraction data. In order to look for the origin of this behaviour the morphology of the RbBr crystallites forming part of the composite under study was carefully inspected for a number of typical powder samples. It was found that most of these crystallites are plate-like in shape with their extended faces perpendicular to one of the crystal ⟨100⟩-directions. In Fig. 7a, showing the LCFE-HREM image of one of the inspected samples, a typical RbBr crystallite may be seen to display this particular morphology. This finding makes feasible to think of the RbBr crystallites in the powder sample to adopt a preferred orientation in the space within the diffractometer sample cup so that their extended faces of the crystallographic form {100} are preferably parallel to the main plane of this cup. Such a preferred orientation may be responsible for the observed differences in relative intensity between the experimental XRD pattern and the standard diffraction data contained in Table 2. It is worth to mention that no plate-like morphology was observed for the crystallites assigned to phases B and T. From the interplanar distance measurements shown in Table 2, an empirical unit-cell size of 6.889 ± 0.007 Å was calculated for phase S, in agreement with the ICDD-PDF-unit-cell size [31] of RbBr. Some other observed reflections (e.g. 1, 2, 5, 8, 9, 11, 13, 15, 17, 18 and 19 in Fig. 2) were properly indexed on the basis of an fcc-phase with a unit-cell size of 7.234 ± 0.025 Å (this phase will be called as phase B from here on in this paper). The assigned indexes as well as the corresponding measured interplanar distances and relative intensities for these reflections are listed in Table 3. Comparison of the measured unit-cell size for phase B with the solid-solution unit-cell-size range limits listed in Table 1 for the binary systems that may in principle be formed from the alkali halides used as precursor salts, shows that from these systems only RbBr:RbI and KI:RbI are compatible in unit-cell size with phase B. From these two systems, the second one was assigned, under the assumption that B is a binary phase (the validity of this assumption is discussed elsewhere), to phase B. This assignation was done by taking advantage of the fact

Table 3 Measured diffraction data and assigned reflection indexes for the binary KI(39%):RbI(61%) phase

Experimental reflection number[a]	Interplanar spacing d (Å)	Relative intensity I_R (%)	Reflection indexes HKL
1	4.19 ± 0.01	7	111
2	3.617 ± 0.008	100	200
5	2.555 ± 0.004	64	220
8	2.179 ± 0.002	5	311
9	2.088 ± 0.002	21	222
11	1.806 ± 0.001	14	400
13	1.617 ± 0.001	25	420
15	1.476 ± 0.001	18	422
17	1.2046 ± 0.0006	7	600
18	1.1424 ± 0.0005	6	620
19	1.0894 ± 0.0005	4	622

[a] In Fig. 2

Table 2 Measured diffraction data for the observed reflections associated to RbBr, and data from the standard diffraction pattern of this salt

RbBr measured diffraction data			RbBr standard diffraction data[a]		
Experimental reflection number[b]	Interplanar spacing d (Å)	Relative intensity I_R (%)	Reflection indexes HKL	Interplanar spacing d_{HKL} (Å)	Relative intensity I_{HKL} (%)
3	3.451 ± 0.007	100	200	3.44	100
6	2.434 ± 0.003	23	220	2.436	75
10	1.992 ± 0.002	14	222	1.989	25
12	1.720 ± 0.001	18	400	1.722	12
14	1.538 ± 0.001	18	420	1.541	25

[a] Reference [31]

[b] In Fig. 2

that, in general, for an ionic fcc-crystal the diffraction relative intensities I_{HKL} with H + K + L odd are particularly sensitive [32] to the cation and anion species forming the crystal. In particular, the observed relative intensity for the reflection 111 of phase B was compared with the ICDD-PDF-I_{111} values [31] of RbBr, RbI and KI, the non-mixed alkali-halide components of the systems RbBr:RbI and KI:RbI. These values, once normalized empirically to each other resulted to be about 0.0, 4.5 and 13.7, respectively, whereas the measured relative intensity for the observed 111-reflection from phase B is about 7 (as shown in Table 3). As normalization factors were used the intensity ratios between the reflections 200 corresponding to the RbBr, RbI and KI salts, as observed in a diffractogram, taken previously for these purposes, of a powder made with equal molar fractions of these salts. As the KI:RbI system satisfies strictly [11] the Vegard's rule, this rule was used to calculate from the measured unit-cell size for phase B the relative concentrations of the KI and RbI components in this phase, resulting to be about 39% and 61%, respectively. The rest of the observed reflections (reflections 4 and 7 in Fig. 2, as well as other four reflections lying behind the silicon 220, 311, 400 and 422-diffraction peaks in this figure) were properly indexed on the basis of an fcc-phase with a unit-cell size of 6.631 ± 0.005 Å (the assigned indexes as well as the corresponding measured interplanar distances and relative intensities are listed in Table 4). This phase, whose probable structure and chemical identity is discussed elsewhere, will be called as phase T from here on in this paper.

Crystal-plate XRD and XRLP

Figure 3 shows a typical crystal-plate X-ray diffractogram of a specimen plate-like in shape that had been mounted on the diffractometer so that one of its extended crystal {100}-faces coincided with the sample-cup main plane. This diffractogram consists of four groups of three reflections each. These groups are indicated as groups I, II, III and IV in the figure. Group I was found to be formed, from the low to the high-angle sides of the diffractogram, by the 200-reflections corresponding to the phases B, S and T, whereas groups II, III and IV were found to be formed by the second, the third and the fourth-order diffraction signals, respectively, of the reflections forming the group I. This finding shows that the S, B and T-crystallites forming the sample have at least one of their respective lattice ⟨100⟩-directions perpendicular to the specimen's crystal {100}-face that was made to coincide with the diffractometer sample-cup main plane. Along this common lattice ⟨100⟩-direction, the Laue-type photograph shown at Fig. 4 was taken. This photograph, displaying a diffraction 4 mm-simmetric pattern of single Laue spots, shows that the crystallites forming the sample, no matter the particular phase they belong to, have in common not only one but all of their respective lattice ⟨100⟩-directions; i.e., that the crystalline composite under study is spatially coherent. However, Fig. 4 also shows that the Laue spots forming the observed diffraction pattern are elongated in

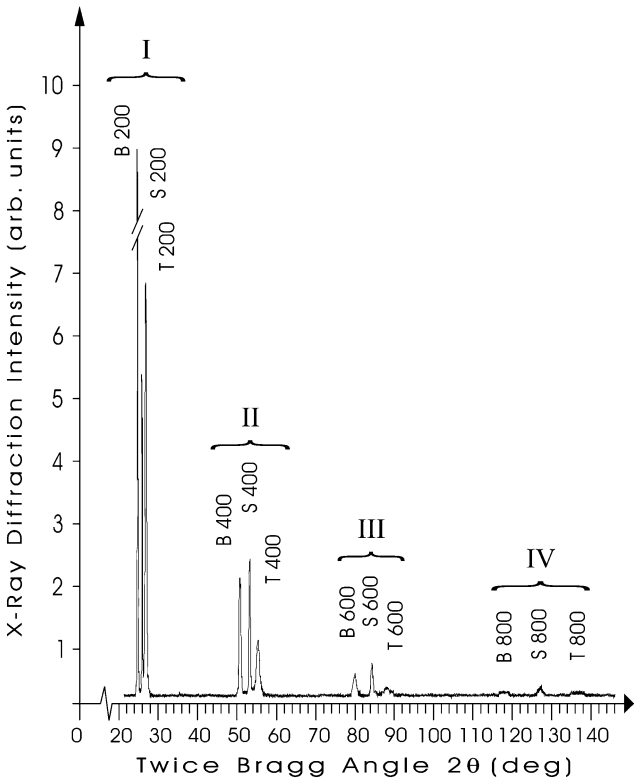

Fig. 3 Crystal-plate X-ray diffractogram of a specimen that was previously mounted on the diffractometer so that one of its extended {100}-faces coincided with the main plane of the sample-cup. The diffractogram consists of four groups (I–IV) of three diffraction peaks each; these peaks correspond to the first, the second, the third and the fourth-order 200-reflections, respectively, corresponding to the phases S, B and T

Table 4 Diffraction data for the observed reflections corresponding to phase T

Reflection indexes HKL	Measured interplanar spacing (Å)	Measured relative intensity I_R (%)
111	3.82 ± 0.01	5
200	3.336 ± 0.007	100
220	2.348 ± 0.003	56
222	1.912 ± 0.002	22
400	1.656 ± 0.001	17
422	1.352 ± 0.001	12
600	1.103 ± 0.001	5

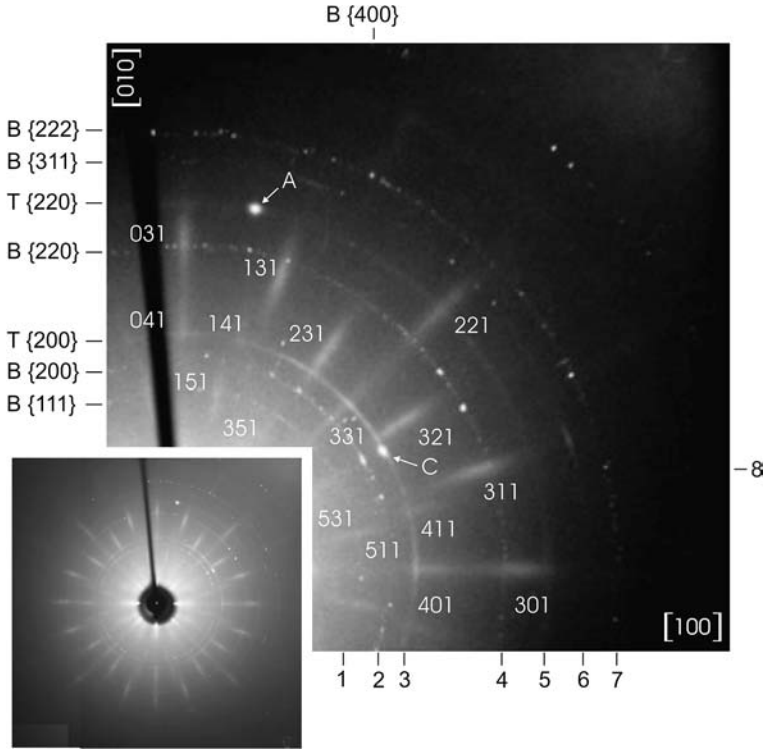

Fig. 4 Transmission Laue photograph taken along the common [001]-lattice direction of the composite, showing a 4 mm-symmetric pattern of elongated Laue spots. An enlarged section of the pattern, once indexed, is also shown. This section shows some incipient Debye rings (1–8). The rings due to the B-phase {HKL}-lattice planes (B{HKL}) are formed by small Bragg spots, whereas the rings due to the T-phase {HKL}-lattice planes (T{HKL}) are formed by short Debye arcs. Two big Bragg spots are also conspicuous (A and C) in the photograph

shape towards the direct-beam spot. This effect, known [33] as radial asterism, has been associated to the use [34, 35] of a conical-convergent X-ray incident beam or well to either [36] crystallite disorientation or crystal bending. As the used incident beam was empirically found to be free of any significant optical convergence the observed asterism was taken as an experimental evidence of the presence of certain crystallographic texture in the composite under study. In order to characterize this texture, the obtained Laue-type patterns were first indexed following standard stereographic-projection procedures [37]. A quarter section of the pattern shown in Fig. 4 is also shown, once indexed, in this figure. Then, the position θ_{HKL}, length M_{HKL} and width N_{HKL} of the observed HKL-Laue spots were measured (listed in Table 5) and then used to build a graph (shown in Fig. 5) by plotting the ratio N_{HKL}/M_{HKL} against θ_{HKL} in radians. This graph showed that the plotted variables are linearly correlated to each other, indicating [38] that the crystallites responsible for the observed elongated HKL-Laue spots are so oriented in the space that the normal to a particular set of reflecting lattice (HKL)-planes describes a narrow cone (the HKL-cone from here on

Table 5 Measured Bragg angles, spot lengths and spot widths for some of the observed HKL-Laue spots, together with the corresponding semiapical angles ϵ_{HKL} of the circular cones confining in the space the normal vectors to the lattice (HKL)-planes of different crystallites

Laue indexes HKL	Measured Laue spots data*			Measured semiapical angles
	Bragg angle θ_{HKL} (±0.008 radians)	Spot length M_{HKL} (±0.2 mm)	Spot width N_{HKL} (±0.2 mm)	ϵ_{HKL} (=360°M_{HKL}/8πD) (±0.05°)
301	0.317	7.7	1.3	2.21
401	0.247	6.0	1.0	1.72
311	0.273	7.6	1.1	2.18
411	0.242	9.1	0.8	2.61
511	0.185	5.7	0.9	1.64
321	0.255	7.0	0.9	2.01
221	0.338	9.6	2.0	2.75
331	0.230	6.8	0.7	1.95

* Laue photographs taken along the direction [001] using a specimen-to-film distance D of 50 mm

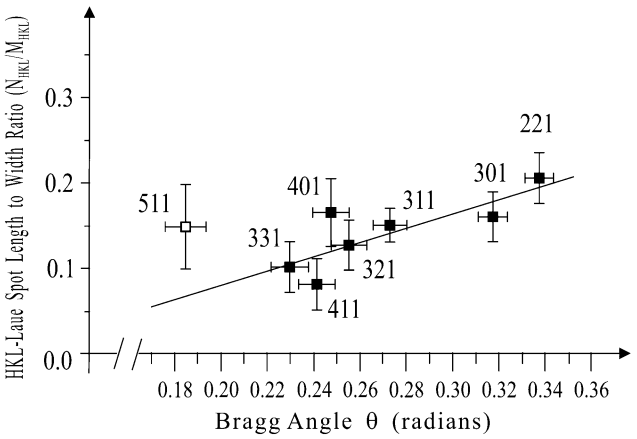

Fig. 5 Plot of the HKL-Laue-spot width-to-length ratio N_{HKL}/M_{HKL} against θ. N and M were determined systematically as the full-width-at-half-maximum values of the profiles, along the spot length and width, respectively, of relative darkness of the spot. The relative darkness of the spot was measured with the help of commercial software, on digitized images of the X-ray diffraction patterns. The data point 511 (plotted with an open centre) was left out, for the reasons explained in the main text, of the least squares fitting analysis performed on the plotted data points. The fitted line, of slop 0.90 ± 0.21, resulting from this analysis is also shown

in this paper) around the lattice [HKL]-direction. In the graph shown Fig. 5, the 511-data point (plotted with an open centre in the figure) is seen to have associated relatively large error bars and also to lie considerably out of the straight line fitted to the rest of data points. This may be due to the fact that the determination of M, N and θ for the Laue spot corresponding to the 511 reflection in Fig. 4 was a compromising matter since this spot lies on the dark region caused by the transmitted beam in the photographic film, and, therefore, is barely visible in the Laue pattern (this situation is extreme in the case of the 531 spot in Fig. 4, and, therefore, M, N and θ were even not determined for this spot). As a result of this fact, the 511-data point in Fig. 5 was not taken into account in the least square fitting analysis of the plotted data in this figure. From this analysis, made by using the experimental error bars as least square fitting weights of the form $1/\text{error}^2$, a slope of 0.90 ± 0.21 was found for the line best fitted. Since this value is consistent with the interpretation [38] of a circular range of crystallite misorientations about each HKL direction, the obtained HKL-cones may be described as circular cones. The semiapical angles ϵ_{HKL} for the 301, 401, 311, 411, 511, 321, 221 and 331-cones were estimated from the M_{HKL} measurements listed in Table 5, by using the approximation [38] $M_{HKL}/4D$, to give the values of (±0.05°) 2.21°, 1.72°, 2.18°, 2.61°, 1.64°, 2.01°, 2.75° and 1.95°, respectively (last column of Table 5).

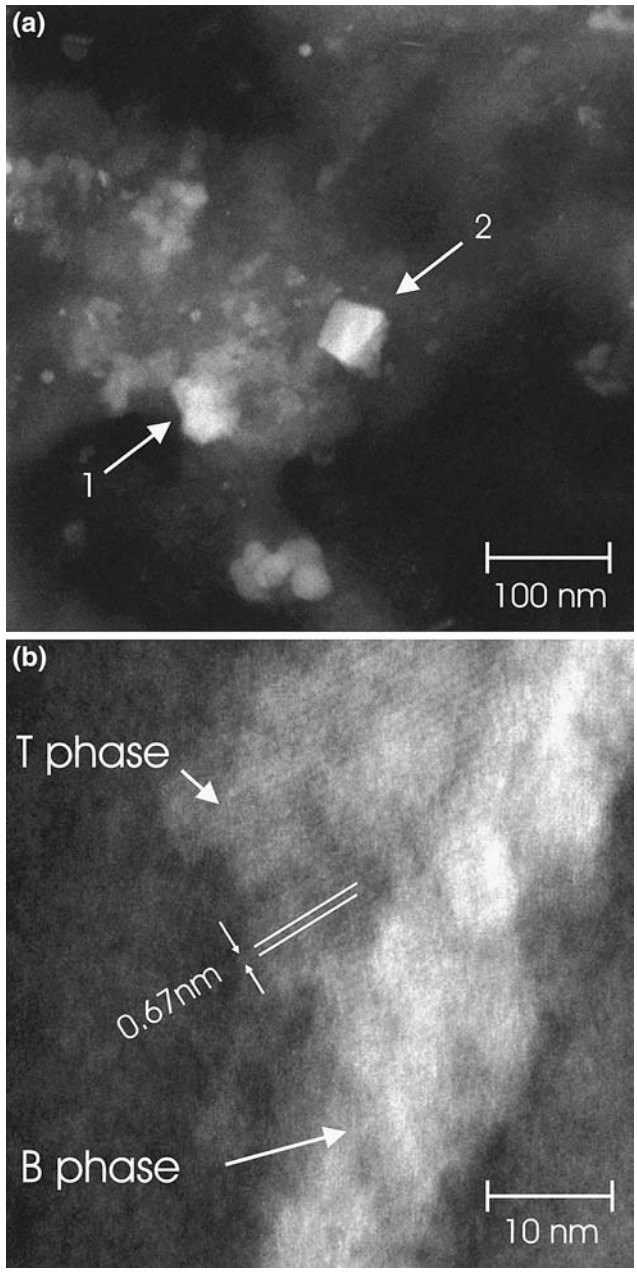

Fig. 6 (**a**) A typical high angle annular dark field image of the sample. In this image, crystallites of the different phases forming the composite appear with different brightness. The brightest crystallites (e.g. 1 and 2) correspond to phase B; (**b**) Higher magnification image showing some zones of B an T-crystallites, as well as some fringes (indicated with white parallel lines) corresponding to phase T

Electron microscopy

Figure 6a and b show typical low and high-magnification high-angle annular dark-field electron micrographs, respectively, of the composite under characterization. As these micrographs were obtained from high-angle electron scattering, crystallites of the

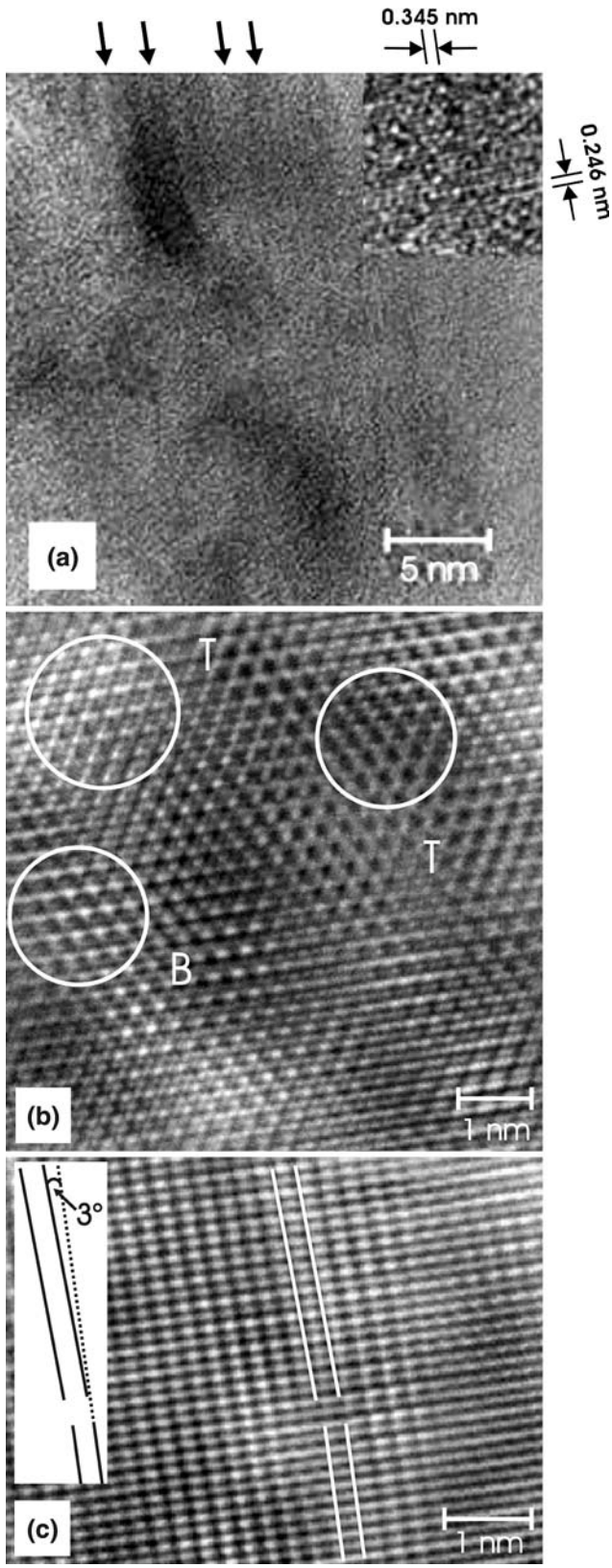

Fig. 7 Typical LCFE-HREM images of the samples, showing: (**a**)▶ a typical RbBr crystallite displaying a plate-like shape with its extended interfaces (perpendicular to the plane of the image and pointed out with arrows at the top of figure) parallel to lattice planes of the form (100). In the inset, showing an enlarged detail of the image, these planes and planes of the form (220) may be seen more clearly, together with their corresponding measured interplanar distances; (**b**) a <111>-view of some zones (encircled in the figure) containing crystallites of the phases B and T, showing that the lattice planes of the crystal {211}-form of these phases are parallel to each other; (**c**) an enlarged view of a detail showing the Moirè pattern formed by the superposition along a common <110>-lattice direction of crystallites of the phases S and T. A typical misfit dislocation between crystallites of these two phases is made evident by using white line segments. A lattice misorientation of about 3° exists (inset) between these crystallites

different phases forming this composite may be observed to appear in the images with different brightness. The brightest crystallites (e.g. crystallites 1 and 2 in Fig. 6a) may be assigned to the binary mixed phase B because of the fact that this phase contains the heavy I^-ions. In Fig. 6b some lattice fringes may be observed to exist (two of them are indicated with white line segments in the figure) in some grey crystallites. For these fringes, a periodicity of about 0.67 nm was measured. This value corresponds to twice the measured lattice (200)-interplanar spacing (as shown in Table 4) for phase T, and, therefore, the grey crystallites in the micrographs were identified as belonging to this phase. For the whole of the observed crystallites, a size distribution in the range from 5 to 60 nm was obtained with an average value of around 13 nm. Figure 7a and b show LCFE-HREM images of two different zones of the sample. In the first image, lattice fringes corresponding to phases S, B and T may be seen to run parallel to each other, confirming that these phases are spatially coherent to each other within the composite. In the second image, showing a view of the B and T-phase crystallites along one of the common <111>-lattice directions (some areas of these phases are encircled in the figure), some lattice {211}-planes of these phases may be seen to be parallel to each other. Long-range lattice modulations due to the introduction of dislocations of the misfit type [39] between crystallites of the different phases were observed to exist in some LCFE-HREM images. In Fig. 7c, showing an enlarged view of a detail once the support amorphous-carbon contribution was removed by image filtering, the Moirè pattern formed by the superposition along a common <110>-lattice direction of the phases S and T may be seen. In this figure, a misfit

dislocation is made evident, by drawing white line segments along the atomic rows. A back of the envelope calculations showed that these dislocations would be separated by about 9 nm. A slight lattice misorientation may also be seen to exist between the crystal lattices of the phases S and T. This misorientation was measured to be of about 3°, in agreement with the crystallographic texture measurements.

Discussion

On the identity of phase B

In order to identify phase B as belonging to the KI:RbI system, the authors assumed previously that phase B is a binary mixed phase. Under this assumption, the authors assigned B to the KI:RbI system on the basis, firstly, of the lattice parameter measured for phase B, and, secondly, of the observed powder X-ray diffraction intensities. The authors could also have assumed that phase B is a ternary phase, instead of a binary one, by including to the proposed binary KI:RbI composition a certain amount of one of the remaining four non-mixed phases (RbCl, KBr, RbBr and KCl) that can in principle be obtained from the ions forming the salts used to prepare the melt. However, as a result of the fact that from these four phases only RbBr satisfies, when compared in unit-cell size with both of the two components of the proposed binary KI:RbI system, the empirical 10%-unit-cell size difference criterion, the composition of a ternary B would be restricted to be KI:RbI:RbBr, which is, under energetic grounds, less probable to form than KI:RbI since both cations and anions have to be exchanged.

On the identity of phase T

As the precursor KBr and RbCl salts were not found to form part, as alkali-halide components, of phase B, they must be present, as alkali-halide components, in phase T. However, as the measured unit-cell size for phase T is higher than the maximum solid-solution unit-cell-size range limit (shown in the last row of Table 1) corresponding to the binary mixed KBr:RbCl system, a third alkali-halide component with a unit-cell size higher than this limit would be required to form part of this phase. From the six different alkali halides that may in principle be obtained by shuffling in pairs the ion species forming the five salts used to prepare the melt, this unit-cell size condition is satisfied only by RbBr, RbI and KI. From these, RbBr keeps the lowest differences in unit-cell size with both KBr and RbCl and, therefore, is probably the third alkali-halide component required to form part of phase T. The authors could also have assumed that phase T is, instead of a ternary phase, a quaternary phase by including to the proposed ternary KBr:RbCl:RbBr composition a certain amount of one of the remaining three non-mixed phases (KI, RbI and KCl,) that can in principle be obtained from the ions forming the salts used to prepare the melt. Under such assumption, as a result of the fact that from these three phases only KI and KCl satisfy, when compared in unit-cell size with all of the three components of the proposed ternary KBr:RbCl:RbBr system, the empirical 10%-unit-cell size difference criterion, the composition of a quaternary T would be KBr:RbCl:RbBr:KI or KBr:RbCl:RbBr:KCl. However, the first of these two quaternary systems is, under energetic grounds, less probable to form than the second one, since cations from three different atom species have to be exchanged in the KBr:RbCl:RbBr:KI-case while cations from only two different atom species have to be exchanged in the KBr:RbCl:RbBr:KCl-case. Therefore, the most probable composition of phase T, under the assumption that this phase is quaternary, would be KBr:RbCl:RbBr:KCl. This last composition and the proposed ternary KBr:RbCl:RbBr composition for phase T are not different from each other from the chemical point of view, since they both contain ions from the same species of chemical elements. So, the authors prefered in this paper to use a ternary, rather than a quaternary, notation for phase T. The existence of the ternary mixed RbBr:KBr:RbCl system, from the point of view of miscibility, has been guaranteed as a limit case by the recently-obtained [26] quaternary mixed KBr:RbCl:RbBr:KCl crystals. The amounts of melt material that could have given place, as a result of crystallization, to each of the three proposed alkali-halide components of phase T were calculated as a first step to compute the probable relative composition of this phase. The T-phase RbCl component must be formed by 20% of the melt material, otherwise the Cl^--ions forming the precursor RbCl salt would have been found in at least one of the other phases (S and B) forming the composite. The T-phase KBr component must share with the B-phase KI component the total amount of the K^+-ions forming the precursor KBr and KI salts otherwise these ions would have been found to form part of phase S or the other component of phase

B. However, as the B-phase KI-component relative concentration was found to be about 39%, even when KI and RbI were used to form the mother melt in equal relative concentrations of 20% (of the melt material) each, about 15.6% [=(39%)(20%/50%)] of the K^+-ions forming the precursor KI salt must form part of the B-phase KI component. The remaining 4.4% (=20–15.6%) of the K^+-ions forming the precursor KI salt must form part of the T-phase KBr component. Therefore, this component must be formed by a total amount of K^+-ions of about 24.4% (=20 + 4.4%) of the melt cationic content, and, consequently, this component must contain about 24.4% of the whole melt material. The melt material percentage (z) forming the T-phase RbBr component is determined by the following two equations, the first one is a stoichiometry-balance equation for phase T, and the second one results from a generalized Vegard's rule for this phase,

$$(24.4\% + 20\% + z)/t = 1$$

$$(24.4\%a1 + 20\%a2 + za3)/t = a\mathrm{T}$$

where a_1, a_2 and a_3 are the unit-cell sizes of KBr, RbCl and RbBr, respectively, a_T is the measured unit-cell size for phase T, and t is a normalization constant. After solving simultaneously the equations given above, z and t resulted to be about 6.72% and 50.72%, respectively. From these values, a relative KBr(47%):RbCl(39%):RbBr(14%) composition may be computed for phase T.

On the departure of the crystallographic texture from a full spatial-coherence condition

Some incipient Debye rings were observed to appear in the inspected Laue-type photographs (e.g. rings 1–8 in Fig. 4). These rings may help to find the structural origin of the observed departure of the composite crystallographic texture from a condition of full spatial coherence. The radii r were measured for these rings and then used to calculate the corresponding angles θ and interplanar distances d (the r, θ and d-values corresponding to the rings 1–8 in Fig. 4 are listed in Table 6). Comparison of these distances with the measured d-data for the phases S, B and T (listed in Tables 2, 3 and 4, respectively) showed that the B-phase {111}, {200}, {220}, {311}, {222} and {400}-lattice planes are responsible for some of the observed rings (rings 1, 2, 4, 6, 7 and 8, respectively, in Fig. 4) while the T-phase {200} and {220}-lattice planes are responsible for the other (rings 3 and 5, respectively, in Fig. 4). The rings associated to phase B may be observed in the inspected Laue-type photographs to be different in structure from the rings associated to phase T. The first are formed by small Bragg spots which may be ascribed [40] to some small randomly-oriented crystallites of phase B adhered as exfoliation remnants to the surface of the specimen, while the others are formed by short Debye arcs passing through some of the observed HKL-Laue spots. The presence of these arcs indicates [38] that there exist, forming part of the composite, some relatively-few T-phase crystallites whose lattice (HKL)-planes are more disoriented than in the rest of the crystallites whatever the phase they belong to. The existence of these highly-disoriented T-phase (HKL)-planes may be taken as an indication of the fact that phase T is the main responsible for the observed asterism, and, therefore, for the observed departure of the composite crystallographic texture from a condition of full spatial coherence.

Conclusions

A novel composite material obtained from a melt prepared by mixing equal molar parts of KBr, RbCl,

Table 6 Measured diffraction data for the observed incipient Debye rings and the crystalline phases and lattice planes that are responsible for these rings

Incipient Debye ring measured diffraction data.				Responsible lattice planes and crystalline phase.	
Ring number[a]	Radius r (±0.010 cm)	Bragg angle θ (°)	Interplanar spacing d (Å)	Lattice planes {HKL}	Crystalline phase[b]
1	1.940	10.603 ± 0.05	4.1857 ± 0.009	111	B
2	2.255	12.137 ± 0.05	3.663 ± 0.006	200	B
3	2.510	13.328 ± 0.05	3.342 ± 0.007	200	T
4	3.475	17.399 ± 0.04	2.576 ± 0.003	220	B
5	3.932	19.090 ± 0.04	2.355 ± 0.003	220	T
6	4.382	20.616 ± 0.03	2.187 ± 0.002	311	B
7	4.677	21.544 ± 0.03	2.098 ± 0.002	222	B
8	6.015	25.132 ± 0.02	1.813 ± 0.001	400	B

[a] In Fig. 4

[b] B stands for KI(39%):RbI(61%) and T stands for KBr(47%):RbCl(39%):RbBr(14%)

RbBr, KI and RbI salts was characterized. This material consists of an aggregation of crystallites, ranging from 5 to 60 nm in size, of three different fcc-phases. One of these phases is identified as single RbBr, another one is discussed to be the binary mixed KI(39%):RbI(61%) phase, and the third one is discussed to be the ternary mixed KBr(47%): RbCl(39%):RbBr(14%) phase. The measured unit-cell sizes for these phases are 6.889 ± 0.007, 7.234 ± 0.025 and 6.631 ± 0.005 Å, respectively. The crystal lattices of the crystallites forming the composite, no matter the particular phase they belong to, are spatially coherent to each other so that the normal vectors to a particular lattice (HKL)-plane, in different crystallites, are confined in the space within a narrow circular cone around the lattice [HKL]-direction. The semiapical angle of this cone depends on (HKL), taking the measured values of (±0.05°) 2.21°, 1.72°, 2.18°, 2.61°, 1.64°, 2.01°, 2.75° and 1.95° for HKL equal to 301, 401, 311, 411, 511, 321, 221 and 331, respectively. The presence of some short Debye arcs in the inspected Laue photographs gives evidences of the fact that the ternary mixed phase crystallites contribute mainly to the observed departure of the composite crystallographic texture from a condition of full spatial coherence.

Acknowledgements The authors wish to thank Prof. José Manuel Hernández for his advice on mixed crystals, Prof. Héctor Riveros Rotge and Mr. Ricardo Guerrero for growing the crystals, Mr. Luis Rendón for his aid on electron microscopy, Mr. R. Unda-Angeles for preparing the figures, Ing. Samuel Tehuacanero for his advice on image treatment and Dr. Miguel Cervantes for taking the picture shown in Fig. 1.

References

1. Bragg WH, Bragg WL (1913) Proc R Soc Lond Ser A 88:428
2. Bragg WL (1913) Proc R Soc Lond Ser A 89:248
3. Glocker R (1914) Phys Zeitschr 15:401
4. Glocker R (1915) Ann D Phys 47:377
5. Hull AW (1919) Trans Am Inst Electr Eng 38:1445
6. Davey WP (1921) Phys Rev 17:402
7. Wyckoff RWG (1921) J Washington Acad 11:429
8. Posnak E, Wyckoff RWG (1922) J Washington Acad 12:248
9. Raynor GV (1958) In: Progress in metal physics, vol 1. Pergamon Press, London, pp 61–62
10. Friedel J (1955) Phil Mag 46:514
11. Sirdeshmukh DB, Srinivas K (1986) J Mater Sci 21:4117
12. Kitaigorodsky AI (1984) In: Mixed crystals. Springer-Verlag, Berlin, pp 181–188, Ch 9
13. Ohno T (1988) J Cryst Growth 91:576
14. Smakula A, Maynard NC, Repucci A (1963) Phys Rev 130(1):13
15. Vegard L, Schjelderup H (1917) Phys Z 18:93
16. Vegard L (1921) Z Phys 5:17
17. Smakula A, Maynard NC, Repucci A (1963) Phys Rev 130:113
18. Mijangos RR, Ruiz-Mejia C (1989) Phys Rev B 39:11120
19. Clark A, Pérez R, Aceves R, Hernández J, Rubio J (1987) Cryst Latt Def Amorph Matt 14:91
20. Pedrero EN, Hernandez JA, Orozco EM, Murrieta HS (1996) Rad Eff Def Sol 138:277
21. Aguilar AM, Benitez F, Verdiguel H, Aguilar GS, Camarillo E, Hernandez JA, Cabrera EB, Murrieta HS (1998) Rad Eff Def Sol 145:233
22. Perez Salas R, Aceves R, Rodriguez-Mijangos R, Riveros HG, Duarte C (2004) J Phys Condensed Matt 16:491
23. Jankowska-Frydel A, Kuklinski B, Nowosielski T, Grinberg M (2001) Rad Measurements 33:773
24. Cordero-Borboa AE, Flores CJ, Hernández JA, Aguilar GS, Murrieta HS (2005) Rad Eff Def Sol 160:121
25. Mijangos RR, Cordero-Borboa A, Camarillo E, Riveros H, Castaño VM (1998) Phys Lett A 245:123
26. Mijangos RR, Riveros H, Camarillo E, Guerrero R, Atondo M, Alvarez E, Rodriguez-Soria A (2000) Phys Stat Sol B 220:687
27. Mijangos RR, Cordero-Borboa A, Alvarez E, Cervantes M (2001) Phys Lett A 282:195
28. Mijangos RR, Alvarez E, Perez-Salas R, Duarte C (2004) Opt Mater 25:279
29. Mijangos RR, Riveros H, Alvarez E, Atondo M, Vazquez-Polo G, Gonzalez GM (2003) Rad Eff Def Sol 158:513
30. Czochralski J (1918) Z Phys Chem 92:219
31. ''Powder Diffraction File'' (International Centre for Diffraction Data, Pennsylvania, USA, 2001) data cards 36-1471, 6-0289, 8-0480, 4-0471 and 6-0218
32. Cullity BD, Stock SR (2001) In: Elements of X-ray diffraction, 3rd ed. Prentice-Hall, Inc, New Jersey, USA, p 141
33. Brasseur H (1947) In: Les Rayons X et leurs applications. Masson et Cie, Editeours, Paris, France, pp 281–283
34. Amorós JL, Buerger MJ, Canut De Amorós M (1975) In: The Laue method. Academic Press, Inc Ltd, London, UK, p 335
35. Azároff LV (1968) In: Elements of X-ray crystallography. McGraw Hill, Inc, New York, USA, pp 395
36. Barret ChS (1952) In: The structure of metals, 2nd ed. McGraw Hill, Inc., New York, USA, p 415
37. Garrido J, Orland J (1946) In: Los Rayos X y la Estructura Fina de los Cristales. Editorial Dossat SA, Madrid, Spain, pp 129–138
38. Cullity BD (1978) In: Elements of X-ray diffraction, 2nd ed. Addison-Wesley Co Inc, Massachusetts, USA, pp 262–264
39. Sutton AP, Baluffi RW (1995) In: Interfaces in crystalline materials. Clarendon Press, Oxford, UK, p 112
40. Wood EA (1963) In: Crystal orientation manual. Columbia University Press, New York, USA, p 73